Journal Pre-proof

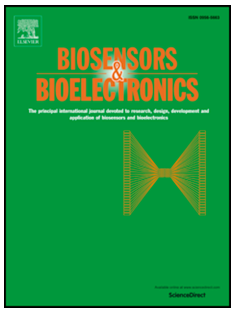

An ultrasensitive biosensor for colorimetric detection of *Salmonella* in large-volume sample using magnetic grid separation and platinum loaded zeolitic imidazolate Framework-8 nanocatalysts

Lei Wang, Xiaoting Huo, Lingyan Zheng, Gaozhe Cai, Yuhe Wang, Ning Liu, Maohua Wang, Jianhan Lin

PII: S0956-5663(19)30941-8

DOI: https://doi.org/10.1016/j.bios.2019.111862

Reference: BIOS 111862

To appear in: *Biosensors and Bioelectronics*

Received Date: 6 August 2019

Revised Date: 4 November 2019

Accepted Date: 7 November 2019

Please cite this article as: Wang, L., Huo, X., Zheng, L., Cai, G., Wang, Y., Liu, N., Wang, M., Lin, J., An ultrasensitive biosensor for colorimetric detection of *Salmonella* in large-volume sample using magnetic grid separation and platinum loaded zeolitic imidazolate Framework-8 nanocatalysts, *Biosensors and Bioelectronics* (2019), doi: https://doi.org/10.1016/j.bios.2019.111862.

An Ultrasensitive Biosensor for Colorimetric Detection of *Salmonella* in Large-volume Sample Using Magnetic Grid Separation and Platinum Loaded Zeolitic Imidazolate Framework-8 Nanocatalysts

Lei Wang[1], Xiaoting Huo[2], Lingyan Zheng[2], Gaozhe Cai[2], Yuhe Wang[2], Ning Liu[2], Maohua Wang[1,2], Jianhan Lin[1,2*]

[1]Key Laboratory of Agricultural Information Acquisition Technology, Ministry of Agriculture and Rural Affairs, China Agricultural University, Beijing 100083, China

[2]Key Laboratory of Modern Precision Agriculture System Integration Research, Ministry of Education, China Agricultural University, Beijing 100083, China

*Corresponding author: Dr. Jianhan Lin, Phone/Fax: +86-10-62737599; Email: jianhan@cau.edu.cn

Abstract

Salmonella is the leading risk factor in food safety. Rapid, sensitive and accurate detection of *Salmonella* is a key to prevent and control the outbreaks of foodborne diseases caused by *Salmonella*. In this study, we reported a colorimetric biosensor for ultrasensitive detection of *Salmonella* Typhimurium using a magnetic grid separation column to efficiently separate target bacteria from large volume of sample and platinum loaded zeolitic imidazolate framework-8 (Pt@ZIF-8) nanocatalysts to effectively amplify biological signal. The target *Salmonella* cells in large volume of sample were first separated and concentrated using the magnetic grid separation column with immune magnetic particle chains, then conjugated with the immune Pt@ZIF-8 nanocatalysts to mimic peroxidase for catalysis of hydrogen peroxide-3,3',5,5'-tetramethylbenzidine, and finally determined by measuring the catalysate at characteristic wavelength of 450 nm. This proposed biosensor was able to separate ~70% of target *Salmonella* cells from 50 mL of bacterial sample and quantitatively detect *Salmonella* from 10^0 to 10^4 CFU/mL in 2.5 h with the lower detection limit of 11 CFU/mL. The mean recovery for *Salmonella* in spiked chicken carcass was about 109.8%. This new magnetic grid separation method was first time reported for efficient separation of target bacteria from very large volume of sample to greatly improve the sensitivity of this biosensor and could be used with various biosensing assays for practical applications in routine detection of foodborne pathogens without any bacterial pre-enrichment.

Key words: Colorimetric biosensor; magnetic particle chain; magnetic grid separation; large-volume sample; Pt@ZIF-8

1. Introduction

Salmonella is the leading risk factor in food safety and its contaminations may occur at any link of the whole food supply chains. Rapid and accurate screening of *Salmonella* has been a key measure to prevent and control the outbreaks of foodborne diseases. Traditional methods for bacteria detection mainly include culture, polymerase chain reaction and enzyme-linked immunosorbent assay, however these methods either are time-consuming, or require complex sample pretreatment, or lack sufficient sensitivity (Kwon et al. 2019; Kwon et al. 2017; Li et al. 2019b; Wang et al. 2019a; Wang and Salazar 2016). Therefore, there is an urgent need for reliable and accurate methods for rapid and sensitive detection of foodborne bacteria.

Enormous efforts have been made on the development of cutting-edge technologies, such as various biosensors for bacteria detection and magnetic separators for bacteria separation (Lee et al. 2019; Schaumburg et al. 2019; Zeinhom et al. 2018). Optical biosensors, relying on the measurement of absorbance, fluorescence, luminescence or scattering, are often featured with easy readout, contactless detection and uncomplicated instrumentation and have become a powerful analytical tool (Dong et al. 2019; Vellaisamy et al. 2018; Wang et al. 2019b; Wu et al. 2019). Due to the complexity of food matrix and extremely low concentration of pathogenic bacteria in routine screening, immunomagnetic separation using magnetic nanoparticles (MNPs) has been widely used in the past decade and become essential for food sample pretreatment (Chattopadhyay et al. 2019; Garrido-Maestu et al. 2019; Iranmanesh and Hulliger 2017; Li et al. 2019a; Schaumburg et al. 2019). However,

this conventional magnetic separation method has obvious limitations, such as low sample handling capability (volume often ≤ 1 mL), high magnetic field requirement, and well-trained technician. Thus, some emerging magnetic separation methods, such as high gradient magnetic separation (HGMS) (Lu et al. 2018; Ryumae et al. 2010, 2012), magnetophoretic separation (MPS) (Guo et al. 2015; Jeong and Lim 2018; Wang et al. 2016) and magnetic flow separation (MFS) (Jung et al. 2018; Lee et al. 2014), were attempted to specifically separate target bacteria from large volume of sample, however HGMS was easily blocked by large-sized particles in food matrix, and MPS required a large amounts of immune MNPs to react with target bacteria in advance. Although MFS was able to continuous-flow separate target bacteria, it was often used at a low flow rate in a microfluidic channel to ensure efficient capture of target bacteria, leading to long separation time or less sample volume. Recently, some interesting studies on the forming of magnetic particle chains were reported for cell sorting, separation and pre-enrichment (Mohamadi et al. 2015; Saliba et al. 2010). The combination of magnetic particle chains with magnetic flow separation might be promising to develop efficient and cost-effective methods for continuous-flow separation of target bacteria from large volume of sample in short time. To the best of our knowledge, there is no study that has reported for rapid, cost-effective and specific separation of foodborne bacteria from very large volume of sample.

Signal amplification is another effective strategy to improve the sensitivity of biosensors. Enzymes are frequently used to amplify biological signals, which are relatively expensive and often featured with poor environmental tolerance and

unsatisfied stability (Huang et al. 2018; Liu et al. 2018; Sun et al. 2019). In recent years, various nanocatalysts with mimic enzyme properties were employed for the development of biosensor due to their merits of lower cost, better stability and tunable catalytic activity (Borghei et al. 2018; Tan et al. 2019; Wang et al. 2018; Xie et al. 2019). Among them, platinum (Pt) nanoparticles with excellent chemical stability, biological compatibility and catalytic activity were often considered as a promising candidate for natural peroxidases (Bu et al. 2019; Cheng et al. 2017; Draz et al. 2018; Wang et al. 2019c; Zhu et al. 2018). Besides, some new nanocarriers with high specific surface and strong load capacity, such as zeolitic imidazolate framework-8 (ZIF-8), graphitic carbon nitride, carbon nanotubes, etc., were reported to increase the load of Pt nanoparticles for enhancing HRP-mimic catalytic reaction, resulting in further improvement on the sensitivity of biosensors (Dai et al. 2019; Ertan et al. 2016; Lian et al. 2017; Liang et al. 2015; Medetalibeyoğlu et al. 2018; Tolga Çolak et al. 2016; Wang and Ma 2019; Yola and Atar 2017).

In this study, a colorimetric biosensor was developed for ultrasensitive detection of *Salmonella* using a magnetic grid separation column for continuous-flow separation of *Salmonella* from large volume of sample and platinum loaded ZIF-8 nanocatalysts for efficient amplification of biological signal. As shown in Fig. 1 and Fig. S1, the immune magnetic particles were first injected into the separation column and formed into magnetic particle chains around the tips of the ring iron grids in the fluidic channel. Then, the *Salmonella* cells in large volume (50 mL) of sample were continuous-flow injected into the column and specifically captured by the

anti-*Salmonella* antibodies on the magnetic particle chains. After the immune Pt@ZIF-8 nanocatalysts were synthesized as signal amplification tags and injected into the column, they were conjugated with the target cells and used to catalyze hydrogen peroxide-3,3',5,5'-tetramethylbenzidine (H_2O_2-TMB), which was terminated using 50 μL of 1 M H_2SO_4 for 1 min. Finally, the catalysate was measured at characteristic wavelength of 450 nm to determine the concentration of *Salmonella*.

Fig. 1

2. Materials and methods

2.1 Materials

The biotinylated polyclonal antibodies (~2.0 mg/mL) against *Salmonella* Typhimurium from Abcam (ab69255, Cambridge, UK, Specificity: react with *Salmonella* sp. in bacterial and infected tissue samples, Purity: Protein A purified.) and the monoclonal antibodies (~3.4 mg/mL) against *Salmonella* Typhimurium from Meridian (Cincinnati, OH, US) were used to separate and label the target *Salmonella* cells, respectively. Zinc acetate dehydrate from Aladdin (Shanghai, China) and dimethylimidazole from Sigma Aldrich (St. Louis, MO, US) were used to synthesize the zeolitic imidazolate framework-8. Chloroplatinic acid ($H_2PtCl_6 \cdot 6H_2O$) from Sigma Aldrich was used to synthesize the platinum nanoparticles. Anhydrous potassium carbonate (K_2CO_3) from Beijing Chemical Reagents (Beijing, China) was used to adjust the pH. Hydrogen peroxide-3,3',5,5'-tetramethylbenzidine from Solarbio (Beijing, China) was used as the catalytic substrate. The carboxylated

magnetic particles (MPs, ~10 mg/mL) with different sizes of ~180 nm, ~600 nm and ~1000 nm from So-Fe Biomedicine (Shanghai, China) were used to magnetically separate the target bacteria. Streptavidin from Hualan Chemical (Shanghai, China), 1-(3-Dimethylaminopropyl)-3-ethylcarbodiimide hydrochloride (EDC·HCl) from D&B Biological (Shanghai, China), and N-Hydroxysulfosuccinimide sodium (NHSS) from Yanye Biotech (Shanghai, China) were used to modify streptavidin onto the MPs. Bovine serum albumin (BSA) from Sigma Aldrich was used for blocking (1% and 10%, w/v). Deionized water was produced by Millipore Advantage 10 (18.2 MΩ·cm, Billerica, MA, US) and used to prepare all aqueous solutions. The concentrated phosphate buffered saline (PBS) from Sigma Aldrich was 10 times diluted with deionized water and used as buffer solution. Other reagents were of analytical grade and obtained from Beijing Chemical Reagents.

2.2 Fabrication of immunomagnetic grid separation column

The immunomagnetic grid separation column is the most important component of this biosensor and has obvious impact on its sensitivity. As shown in Fig. 1, it was composed of an inner glass tube (inner diameter: 4.4 mm, outer diameter: 6.0 mm, length: 55 mm), an outer glass tube (inner diameter: 7.0 mm, outer diameter: 9.0 mm, length: 65 mm) and a ring iron hoop (inner diameter: 9.2 mm, outer diameter: 10.0 mm, length: 55 mm). Different thickness (2.0 mm, 4.0 mm, 6.0 mm and 8.0 mm) of cylinder magnets (material: NdFeB; grade: N52; diameter: 4.0 mm) were mutually repelled in the inner glass tube and each two adjacent magnets were separated by an

ring iron grid (diameter: 4.3 mm; thickness: 0.5 mm) to generate local high gradient magnetic fields at the tips of the grid. After each end of the inner tube was connected with an aligner, which was fabricated by a 3D printer (Object 24, Stratasys, Eden Prairie, MN, US), it was inserted into the outer tube to make the tubes concentric, resulting in the forming of a ring fluidic channel (inner diameter: 6.0 mm, outer diameter: 7.0 mm). As shown in Fig. S2, the aligner was improved based on our previous design (Wang et al. 2017) to allow the solutions to flow through the fluidic channel more uniformly by removing five symmetric arc-cylinders (arc angle: 45^{o}, height: 0.4 mm) from the cylinder and avoid the residuals by adding one triangle cone (diameter: 6.0 mm, height: 3.0 mm). The iron hoop was set over the outer tube and aligned with the inner tube to control the magnetic field lines for better forming of magnetic particle chains in the fluidic channel. Finally, each end of the outer glass tube was connected with a silicone hose via a 3D-printed connector. The silicone hose was installed on the peristaltic pump (T60-S2&WX10-14-A, Longer, Baoding, China) for accurate liquid operations. The distribution of the magnetic field in this separation column was simulated by the Finite Element Method Magnetics (FEMM) Software.

2.3 Modification of immune magnetic particles

The immune magnetic particles (IMPs) with different sizes of 180 nm, 600 nm and 1000 nm were prepared using the EDC/NHSS method and compared in this study to specifically separate the target bacteria from large volume of samples. First, 2 mg of carboxyl functionalized MPs were washed with 1 mL of PBS three times and

resuspended in 1 mL of PBS. Then, EDC·HCl (0.58 mg, 0.17 mg and 0.10 mg) and NHSS (0.65 mg, 0.20 mg and 0.12 mg) were freshly prepared in PBS (0.01 M, pH 7.4) and used to activate carboxyl groups for 1 h at 15 rpm, respectively. After washing with PBS three times, the MPs were incubated with 0.16 mg of streptavidin in 1 mL of PBS at 37°C for 2 h at 15 rpm respectively, followed by blocking with 100 μL of 10% BSA for 45 min. Finally, the streptavidin modified MPs were conjugated with 100 μg of biotinylated polyclonal antibodies at 15 rpm for 45 min respectively, allowing the forming of the IMPs through streptavidin-biotin binding, and magnetically separated to remove surplus antibodies.

2.4 Synthesis of platinum loaded ZIF-8 nanocatalysts

Zeolitic imidazolate framework-8 was synthesized according to previous study with some modifications (Wu et al. 2015). First, 2.4 mL of 0.3 M zinc acetate dehydrate was mixed uniformly with 9 mL of 0.8 M dimethylimidazole at 15 rpm for 1 h. Then, the white precipitates were collected by centrifuging at 6,000 rpm for 10 min and washing with deionized water three times to remove residual reagents. Finally, the ZIF-8 powder was obtained by baking at 37°C for 12 h and stored at 4°C for further use.

The Pt nanoparticles with the diameter of ~5 nm were prepared to mimic horse radish peroxidase (HRP) according to previous study (Bigall et al. 2008). First, 36 mL of chloroplatinic acid hexahydrate (0.2%, v/v) was quickly added into 464 mL of boiling deionized water. Then, 11 mL of aqueous solution (containing 1% sodium

191 citrate and 0.05% citric acid, from Solarbio) and 5.5 mL of freshly prepared sodium
192 borohydride (0.08%, from Aladdin) in ice solution (1% sodium citrate and 0.05%
193 citric acid) were successively added. After incubation for 10 min, the mixture was
194 cooled to room temperature and the synthesized platinum nanoparticles were stored at
195 4°C for further use.

196 The Pt@ZIF-8 nanocatalysts were synthesized based on adsorptive property of
197 ZIF-8. First, the pH of Pt nanoparticles was adjusted to 7.0 with K_2CO_3 (0.2 M). Then,
198 20 mg of ZIF-8 nanoparticles were added and sonicated about 2 min to make them
199 dissolve in the solution. After incubation for 1 h, the Pt@ZIF-8 nanocatalysts were
200 obtained by centrifuging at 10,000 rpm for 5 min and washing three times with
201 deionized water. Finally, the Pt@ZIF-8 nanocatalysts (10 mg/mL) were dispersed in 2
202 mL of deionized water and stored at 4°C for further use.

203 **2.5 Preparation of immune Pt@ZIF-8 nanocatalysts**

204 The Pt@ZIF-8 nanocatalysts were modified with monoclonal antibodies through
205 electrostatic adsorption for labeling target bacteria. First, 10 μg of monoclonal
206 antibodies were incubated with 1 mL of Pt@ZIF-8 nanocatalysts (10 mg/mL) for 1 h.
207 Then, 100 μL of 10% BSA was added drop-by-drop to block surplus sites for 30 min,
208 and the immune Pt@ZIF-8 nanocatalysts were obtained by centrifuging at 10,000 rpm
209 for 5 min and washing three times with deionized water. Finally, the immune
210 Pt@ZIF-8 nanocatalysts (10 mg/mL) were dispersed in 1 mL of deionized water
211 containing 1% BSA and stored at 4°C for further use.

2.6 Detection of target bacteria in pure culture

To prove the concept of efficient separation and sensitive detection of target bacteria, 50 mL of target bacterial samples with different concentrations ranging from 1.3 x 10^0 to 1.3 x 10^4 CFU/mL were prepared and detected using this biosensor. Prior to testing, the magnetic grid separation column was washed with alcohol and deionized water respectively, and blocked with 1% BSA for 30 min. First, 200 μg of IMPs in 1 mL of PBS were injected into the column at a flow rate of 5 mL/min to form immune magnetic particle chains around the iron grid. Then, 50 mL of target bacterial sample at each concentration was injected into the column and the target bacteria were captured by the antibodies onto the immune magnetic particle chains to form MP-bacteria complexes (magnetic bacteria), followed by washing with 5 mL of deionized water at a flow rate of 0.8 mL/min. Successively, 500 μL of immune Pt@ZIF-8 nanocatalysts (2 mg/mL) were injected and incubated with the magnetic bacteria for 45 min to form MP-bacteria-Pt@ZIF-8 complexes (nanocatalyst bacteria). After washing with 5 mL of deionized water, 500 μL of H_2O_2-TMB was used to immerse the nanocatalyst bacteria, followed by incubation for 30 min. Finally, the catalysate was flushed out and the reaction was terminated by 50 μL of 1 M H_2SO_4. The absorbance of the catalysate was analyzed and measured by the microplate reader (Infinite M200 PRO, Tecan, Austria) at characteristic wavelength of 450 nm to determine the concentration of target bacteria.

2.7 Detection of target bacteria in spiked chicken carcass

The chicken carcass bought from local supermarket was used to mimic real food sample to verify the applicability of this proposed biosensor. First, 250 mL of PBS was used to rinse chicken carcass with vigorous shaking for 5 min. After standing for 10 min to obtain the supernatant, 50 mL of spiked chicken carcass samples with bacterial concentrations from 1.3 x 10^0 to 1.3 x 10^4 CFU/mL were prepared by adding different concentrations of target bacteria to the supernatant. Finally, the spiked samples were detected using the proposed biosensor according to the protocol described in Section 2.6.

3. Results and Discussion

3.1 Mechanism of magnetic particle chain forming

The forming of magnetic particle chains is vital to efficient separation of target bacteria from large volume of sample. In theory, magnetic particles in a magnetic field move from lower gradient zone to higher one along magnetic field lines, and finally aggregate at the highest gradient zone. Thus, it is very important to investigate force analysis of the magnetic particles in the fluidic channel at the presence of external magnetic field for better understanding forming mechanism of magnetic particle chains. As shown in Fig. S3, four forces act on a magnetic particle including magnetic force ($\boldsymbol{F_m}$), fluidic push ($\boldsymbol{F_p}$), gravity ($\boldsymbol{F_g}$) and floatage ($\boldsymbol{F_f}$). In this study, compared to the magnetic force (~ 10^{-10} N), the gravity (~ 10^{-14} N) and the floatage (~ 10^{-15} N) are much smaller and can be ignored. Thus, the trajectory of magnetic particle is

dominated by the magnetic force and influenced by the fluidic push (~ 10^{-11} N). If the fluidic push was not present, the magnetic particle would move along its original magnetic field line (L_1) to the highest gradient zone. However, when the fluidic push is present, it makes the magnetic particle move across the magnetic field lines (from L_1 to L_4), not completely following the original one (see Fig. S3). Right before the moving magnetic particle (black) hits the fixed one (blue) that has been captured in the highest gradient zone (at the moment of t-Δt), the fluidic push and the magnetic force with the same direction as the magnetic field line (L_3) act on the moving particle, making it move towards the fixed one. When the moving particle is hitting the fixed one (at the moment of t), the counter force ($\boldsymbol{F_c}$) starts to act on the moving particle with the reverse direction as the magnetic field line (L_4) while the direction of magnetic force is still unchanged (L_3) due to magnetic hysteresis, resulting in a combined force with the upward direction. The combined force will quickly make the particle move upwards and finally reach a balance at the moment of t+Δt. Thus, when the magnetic particles are continuous-flow flowing through the fluidic channel, they will be captured and formed into chains at the magnetic grid zone.

3.2 Simulation of magnetic field in fluidic channel

The magnetic field distributed in the fluidic channel of the magnetic grid separation column is the key to successful forming of magnetic particle chains and thus has great impact on separation efficiency of target bacteria. Since the magnetic particle chains standing vertically in the fluidic channel can obviously increase the

opportunities for the antibodies on the magnetic particles to capture the flowing target bacteria, it is important to make the magnetic field be vertical to the flow direction.

Because the magnetic field lines always go the way with the least magnetic resistance, the iron hoop was set over the outer tube to control the magnetic field lines. To verify this, the magnetic field with and without the iron hoop was simulated and analyzed using the FEMM software. As shown in Fig. 2a, when the iron hoop is present, much more magnetic field lines go through the fluidic channel vertically, indicating that the magnetic particles are easier to form the chains with the iron hoop than without the iron hoop. Besides, the magnetic intensity in the fluidic channel at each tip of the iron grid (from the inner point A to the outer point B) for the magnetic fields with the hoop and without the hoop is shown in Fig. 2b. Their mean magnetic gradients are basically the same, however the mean magnetic intensity with the iron hoop (0.66 T) is higher than that without the iron hoop (0.54 T). To further verify this, three parallel tests on continuous-flow separation of 50 mL of target bacteria with the concentration of 1.7×10^3 CFU/mL were conducted using the magnetic grid separation column with and without the iron hoop (the length of the magnets: 8 mm). As shown in Fig. 2c, the separate efficiency (72.1%, defined as the ratio of the amount of the captured bacteria to that of the original one) of the target bacteria with the iron hoop is obviously higher than that (50.7%) without the iron hoop, further verifying the effectiveness of the iron hoop.

The length of the magnet is also important in the development of the magnetic field. Since the magnetic resistance of the iron hoop is very small compared to the air

297 and the glass and can be ignored, the length of the magnets (D_1) should be obviously
298 larger than 2 times of the distance (D_2) between the tip of the iron grid and the inner
299 wall of the iron hoop, i.e., only when D_1 is much larger than $2D_2$, most magnetic field
300 lines will go through the fluidic channel vertically due to the smaller magnetic
301 resistance. To verify this, the magnetic fields with different lengths of magnets and the
302 same iron grid and iron hoop were simulated using the FEMM software. As shown in
303 Fig. 2d-e, when the length of the magnet changes from 2 mm to 8 mm, the number of
304 the vertical magnetic field lines (the angle between the line and the flow direction
305 larger than 45°) passing through the fluidic channel in the red rectangle region
306 increases from 2 to 12, and the mean magnetic intensity increases from 0.17 T to 0.76
307 T with the same magnetic gradient of 320 T/m. The further increase in the length of
308 the magnet results in less change on the number of the magnetic field lines and the
309 magnetic intensity. Therefore, the optimal length of 8 mm for the magnet was used in
310 this study.

311 Besides, the thickness of the iron grid was also investigated to understand the
312 effect on the magnetic field lines. As shown in Fig. S4, for different thicknesses of
313 iron grids, the number of the magnetic field lines, the mean magnetic intensity (~ 0.7
314 T) and gradient (~ 300 T/m) of the magnetic field are basically consistent, indicating
315 that the thickness of iron grids has little effect on the magnetic field lines. Therefore,
316 the thickness of 0.5 mm was used in this study.

Fig. 2

317

318 **3.3 Optimization of magnetic grid separation of target bacteria**

Efficient separation of target bacteria from large volume of sample using the magnetic grid separation column is vital to the sensitivity of the proposed biosensor. To select the best magnetic particles for this study, 200 μg of IMPs with different sizes of 180 nm, 600 nm and 1000 nm were compared and used to separate target bacteria with the concentration of 1.9 x 10^3 CFU/mL from 50 mL of bacterial sample. As shown in Fig. 3a, with the increase of the size of IMPs, the separation efficiency increases from 49.0% to 70.7%. This is mainly due to the forming of more magnetic particle chains in the fluidic channel for larger sized IMPs, resulting in the capture of more target bacteria. Therefore, the IMPs with optimal size of 1000 nm were used in this study.

Besides, the flow rate of the bacterial sample also has impact on separation of target bacteria. Thus, different flow rates of 0.4 mL/min, 0.8 mL/min, 1.2 mL/min and 1.5 mL/min were used to separate target bacteria with the concentration of 2.3 x 10^3 CFU/mL from 50 mL of bacterial sample. As shown in Fig. 3b, the separation efficiency increases from 44.6% to 68.0%, when the flow rate decreases from 1.5 mL/min to 0.8 mL/min. However, further decrease in the flow rate results in little change (<5%) on the separation efficiency. Therefore, to trade off the separation efficiency and the separation time, the optimal flow rate of 0.8 mL/min was used in this study.

Fig. 3

3.4 Optimization of immune Pt@ZIF-8 nanocatalysts

The immune Pt@ZIF-8 nanocatalysts used as signal amplifying tags are the key to the sensitivity of this proposed biosensor. The load of Pt nanoparticles onto the ZIF-8 nanoparticles has great impact on the amplification of biological signal, so it is essential to understand the load capacity of ZIF-8 nanoparticles. The same amount (20 mg) of ZIF-8 nanoparticles were added into different volumes (1 mL, 2 mL, 4 mL and 6 mL) of Pt nanoparticles solution (pH 7.0) to synthesize the Pt@ZIF-8 nanocatalysts (10 mg/mL), which were then evaluated by catalyzing the H_2O_2-TMB substrate. As shown in Fig. 4a, the pure Pt nanoparticles are brown and the pure ZIF-8 nanoparticles are white. When more Pt nanoparticles are absorbed by the ZIF-8 nanoparticles, the color becomes deeper gradually from pure white to black gray. After the Pt@ZIF-8 nanocatalysts were synthesized, 100 μL of them (1 mg/mL) were used to catalyze 100 μL of H_2O_2-TMB for 15 min, respectively. As shown in Fig. 4b, the absorbance at 450 nm increases from 0.50 to 0.91, when the volume of Pt nanoparticles changes from 1 mL to 4 mL. However, further increase in the volume results in little change (<10%) on the absorbance. This might be because the load capacity of ZIF-8 nanoparticles is saturated. Therefore, the optimal volume of 4 mL for Pt nanoparticles was used in this study.

The amount of immune Pt@ZIF-8 nanocatalysts and the time for catalytic reaction are also crucial to the sensitivity of the proposed biosensor. Thus, different amounts of immune Pt@ZIF-8 nanocatalysts were compared for detection of target bacteria with the concentration of 1.3×10^3 CFU/mL. As shown in Fig. 4c, the absorbance at 450 nm increases from 0.37 to 0.83 when the amount of immune Pt@ZIF-8 nanocatalysts

changes from 0.25 mg to 1.0 mg. However, further increase in the amount results in little change (<8%) on the absorbance. Thus, the optimal amount of 1 mg for immune Pt@ZIF-8 nanocatalysts was used in this study. Besides, different time for immune Pt@ZIF-8 nanocatalysts to catalyze the H_2O_2-TMB substrate was also compared for detection of target bacteria with the concentration of 1.3×10^3 CFU/mL. As shown in Fig. 4d, the absorbance increases from 0.45 to 0.84 when the catalytic reaction time changes from 10 min to 30 min, and the absorption for 40 min and 50 min does not increase obviously compared to that for 30 min, indicating that 30 min is sufficient for the Pt@ZIF-8 nanocatalysts to catalyze the substrate. Therefore, the optimal catalytic reaction time of 30 min was used in this study.

Fig. 4

3.5 Characterization of immune Pt@ZIF-8 nanocatalysts

The immune Pt@ZIF-8 nanocatalysts with the HRP mimic enzymatic characteristics play an important role in the development of this proposed biosensor since they act as the signal amplifying tags to improve the sensitivity. To verify the successful synthesis of the nanocatalysts, the Pt nanoparticles, the ZIF-8 nanoparticles, and the Pt@ZIF-8 nanoparticles were characterized using transmission electron microscope (TEM). The TEM imaging results show that the Pt nanoparticles display a uniform and monodispersed spherical morphology with the size of ~ 5 nm (Fig. 5a) and the ZIF-8 nanoparticles are rhombododecahedron with the size of ~ 470 nm (Fig. 5b). As shown in Fig. 5c, a large amount of Pt nanoparticles are observed on the

surface of Pt@ZIF-8 nanoparticles, indicating successful absorption of Pt nanoparticles. Besides, as shown in Fig. 5d, the dynamic light scattering (DLS) results indicate that the diameter of Pt@ZIF-8 nanoparticles (~500 nm) is larger than the pure ZIF-8 nanoparticles (~470 nm) , which are consistent with TEM imaging results. As shown in Fig. 5e, the increase in the volume adsorbed at very low relative pressures indicates the nanoporous structure of the synthesized ZIF-8 nanoparticles. The specific surface area of ZIF-8 nanoparticles is up to 907.4 m^2/g, indicating that the ZIF-8 nanoparticles have a high loading efficiency for Pt nanoparticles. As shown in Fig. 5f, the pore sizes are narrowly distributed between 0.8 nm and 2.0 nm, indicating that the ZIF-8 nanoparticles have a uniform pore structure as well and the Pt nanoparticles are loaded onto the surface of ZIF-8 nanoparticles.

To further prove the concept of this proposed biosensor, different concentrations of Pt@ZIF-8 nanoparticles were used to catalyze the H_2O_2-TMB substrate. As shown in Fig. 5g, the absorbance at 450 nm increases with the concentration of Pt@ZIF-8 nanoparticles, and the absorbance ($\boldsymbol{A}$) has a good linear relationship with the concentration ($\boldsymbol{C_n}$) of Pt@ZIF-8 nanoparticles ranging from 0.025 mg/mL to 1.0 mg/mL, which can be expressed as $\boldsymbol{A} = 0.3244*\ln(\boldsymbol{C_n}) + 1.5662$ (R^2=0.99).

Fig. 5

3.6 Performance evaluation of this proposed biosensor

Under the optimal conditions, the calibration curve between the absorbance and the concentration for this proposed biosensor was established to determine the

concentration of *Salmonella* Typhimurium in an unknown sample. Three parallel tests on pure *Salmonella* cells with different concentrations of 1.3 x 10^0-1.3 x 10^4 CFU/mL were conducted using this proposed biosensor. As shown in Fig. 6a-b, the absorbance at 450 nm increases from 0.30 to 1.21 while the bacterial concentration changes from 1.3 x 10^1 CFU/mL to 1.3 x 10^4 CFU/mL, and a good linear relationship between the absorbance ($\boldsymbol{A}$) and the concentration ($\boldsymbol{C_b}$) is found and can be expressed by: $\boldsymbol{A}$ = 0.1352*ln($\boldsymbol{C_b}$)-0.1172 (R^2=0.98). The low detection limit of this biosensor was determined by 3 times of signal-to-noise ratio to be 11 CFU/mL. This colorimetric biosensor was also compared with some recently reported methods. As shown in Table S1, this proposed biosensor has a higher sensitivity and a comparable detection time. The high sensitivity of this biosensor was mainly contributed to two aspects: (1) effective amplification of biological signals using the Pt@ZIF-8 nanocatalysts as amplifying tags; (2) efficient separation of target bacteria from very large volume (50 mL) of sample using the magnetic particle chains formed in the magnetic grid separation column. Besides, the TEM imaging was used to verify successful forming of MP-bacteria complexes and MP-bacteria-Pt@ZIF-8 complexes (see Fig. 6c), and the microscopy was employed to observe the magnetic particle chains (see Fig. 6d). It can be clearly seen that the magnetic particle chains are successfully formed when the iron hoop is used.

To evaluate the specificity of this proposed biosensor, five common foodborne pathogenic bacteria, including *Staphylococcus aureus*, *Vibrio parahaemolyticus*, *Listeria monocytogenes*, *Bacillus cereus* and *E. coli* O157: H7 with the concentration

of 10^3 CFU/mL were used as non-target bacteria and detected using this biosensor. As shown in Fig. 6e, the absorbance values at 450 nm of negative control, *Staphylococcus aureus*, *Vibrio parahaemolyticus*, *Listeria monocytogenes*, *Bacillus cereus* and *E. coli* O157: H7 are 0.18, 0.33, 0.28, 0.25, 0.29 and 0.18, respectively, and much lower than that of *Salmonella* Typhimurium (0.85) at the same concentration, indicating that this proposed biosensor has a good specificity.

To further evaluate the practical applicability of this proposed biosensor for detection of *Salmonella* Typhimurium in food samples, three parallel tests on different concentrations of the *Salmonella* cells in spiked chicken carcass were conducted using this biosensor. As shown in Fig. 6f, the absorbance at 450 nm for the spiked chicken carcass at each concentration is slightly higher than that for the pure culture at the same concentration. This might be due to the interferences from the chicken sample background, since a large number of proteins, fats and other molecules might influence the separation and detection of the target bacteria. The recoveries for different concentrations of the target bacteria range from 105.4% to 114.4%, with an average of 109.8%. This indicates that the proposed biosensor has a good applicability for detection of *salmonella* Typhimurium in chicken samples.

Fig. 6

4. Conclusions

In this study, we successfully developed a colorimetric biosensor using magnetic grid separation and platinum loaded zeolitic imidazolate framework-8 nanocatalysts for ultrasensitive and rapid detection of *Salmonella*. This biosensor was able to detect

448 *Salmonella* as low as 11 CFU/mL in 2.5 h. The immune Pt@ZIF-8 nanocatalysts were
449 verified with a good peroxidase-like enzymatic activity to catalyze H_2O_2-TMB and
450 could greatly amplify biological signals. More importantly, the magnetic grid
451 separation method was first time demonstrated with a high separation efficiency of
452 target bacteria from a very large volume of sample to greatly improve the sensitivity
453 of this biosensor and could be used with various biosensors or bioassays for biological,
454 chemical and medical applications.
455
456 **Acknowledgments**
457 This study was supported in part by the National Natural Science Foundation of
458 China (31802219), Walmart Foundation (SA17031161) and Walmart Food Safety
459 Collaboration Center. The authors would like to thank Yafang Shen and Qi Zhang at
460 Zhejiang University for their suggestions on the synthesis of ZIF-8.
461
462

References

Bigall, N.C., Hartling, T., Klose, M., Simon, P., Eng, L.M., Eychmuller, A., 2008. Monodisperse platinum nanospheres with adjustable diameters from 10 to 100 nm: synthesis and distinct optical properties. Nano letters 8(12), 4588-4592.

Borghei, Y.S., Hosseini, M., Ganjali, M.R., 2018. Oxidase-like Catalytic activity of Cys-AuNCs upon visible light irradiation and its application for visual miRNA detection. Sensors and Actuators B: Chemical 273, 1618-1626.

Bu, S.J., Wang, K.Y., Bai, H.S., Leng, Y., Ju, C.J., Wang, C.Y., Liu, W.S., Wan, J.Y., 2019. Immunoassay for pathogenic bacteria using platinum nanoparticles and a hand-held hydrogen detector as transducer. Application to the detection of *Escherichia coli* O157:H7. Mikrochimica acta 186(5), 296.

Chattopadhyay, S., Sabharwal, P.K., Jain, S., Kaur, A., Singh, H., 2019. Functionalized polymeric magnetic nanoparticle assisted SERS immunosensor for the sensitive detection of *S.* typhimurium. Analytica chimica acta 1067, 98-106.

Cheng, N., Song, Y., Zeinhom, M.M.A., Chang, Y.C., Sheng, L., Li, H., Du, D., Li, L., Zhu, M.J., Luo, Y., Xu, W., Lin, Y., 2017. Nanozyme-Mediated Dual Immunoassay Integrated with Smartphone for Use in Simultaneous Detection of Pathogens. ACS applied materials & interfaces 9(46), 40671-40680.

Dai, L., Li, Y., Wang, Y., Luo, X., Wei, D., Feng, R., Yan, T., Ren, X., Du, B., Wei, Q., 2019. A prostate-specific antigen electrochemical immunosensor based on Pd NPs functionalized electroactive Co-MOF signal amplification strategy. Biosensors & bioelectronics 132, 97-104.

Dong, J., Chen, J.F., Smalley, M., Zhao, M., Ke, Z., Zhu, Y., Tseng, H.R., 2019. Nanostructured Substrates for Detection and Characterization of Circulating Rare Cells: From Materials Research to Clinical Applications. Advanced materials, e1903663.

Draz, M.S., Lakshminaraasimulu, N.K., Krishnakumar, S., Battalapalli, D., Vasan, A., Kanakasabapathy, M.K., Sreeram, A., Kallakuri, S., Thirumalaraju, P., Li, Y., Hua, S., Yu, X.G., Kuritzkes, D.R., Shafiee, H., 2018. Motion-Based Immunological Detection of Zika Virus Using Pt-Nanomotors and a Cellphone. ACS nano 12(6), 5709-5718.

Ertan, B., Eren, T., Ermis, I., Saral, H., Atar, N., Yola, M.L., 2016. Sensitive analysis of simazine based on platinum nanoparticles on polyoxometalate/multi-walled carbon nanotubes. Journal of colloid and interface science 470, 14-21.

Garrido-Maestu, A., Azinheiro, S., Carvalho, J., Prado, M., 2019. Combination of Immunomagnetic Separation and Real-Time Recombinase Polymerase Amplification (IMS-qRPA) for Specific Detection of *Listeria monocytogenes* in Smoked Salmon Samples. Journal of food science.

Guo, P.L., Tang, M., Hong, S.L., Yu, X., Pang, D.W., Zhang, Z.L., 2015. Combination of dynamic magnetophoretic separation and stationary magnetic trap for highly sensitive and selective detection of *Salmonella* typhimurium in complex matrix. Biosensors & bioelectronics 74, 628-636.

Huang, H., Zhao, G., Dou, W., 2018. Portable and quantitative point-of-care monitoring of *Escherichia coli* O157:H7 using a personal glucose meter based on

immunochromatographic assay. Biosensors & bioelectronics 107, 266-271.
Iranmanesh, M., Hulliger, J., 2017. Magnetic separation: its application in mining, waste purification, medicine, biochemistry and chemistry. Chemical Society reviews 46(19), 5925-5934.
Jeong, A., Lim, H.B., 2018. Magnetophoretic separation ICP-MS immunoassay using Cs-doped multicore magnetic nanoparticles for the determination of *salmonella* typhimurium. Talanta 178, 916-921.
Jung, S.H., Hahn, Y.K., Oh, S., Kwon, S., Um, E., Choi, S., Kang, J.H., 2018. Advection Flows-Enhanced Magnetic Separation for High-Throughput Bacteria Separation from Undiluted Whole Blood. Small 14(34), e1801731.
Kwon, K., Gwak, H., Hyun, K.-A., Kwak, B.-S., Jung, H.-I., 2019. High-throughput microfluidic chip for magnetic enrichment and photothermal DNA extraction of foodborne bacteria. Sensors and Actuators B: Chemical 294, 62-68.
Kwon, K., Park, J.-W., Hyun, K.-A., Kwak, B.S., Yong, D.E., Hwang, J., Jung, H.-I., 2017. Continuous adsorption and photothermal lysis of airborne bacteria using a gold-nanoparticle-embedded-geometrically activated surface interaction (gold-GASI) chip. Sensors and Actuators B: Chemical 248, 580-588.
Lee, C.W., Chang, H.Y., Wu, J.K., Tseng, F.G., 2019. Ultra-sensitive electrochemical detection of bacteremia enabled by redox-active gold nanoparticles (raGNPs) in a nano-sieving microfluidic system (NS-MFS). Biosensors & bioelectronics 133, 215-222.
Lee, W., Kwon, D., Chung, B., Jung, G.Y., Au, A., Folch, A., Jeon, S., 2014. Ultrarapid Detection of Pathogenic Bacteria Using a 3D Immunomagnetic Flow Assay. Analytical Chemistry 86(13), 6683-6688.
Li, J., Liu, Q., Wan, Y., Wu, X., Yang, Y., Zhao, R., Chen, E., Cheng, X., Du, M., 2019a. Rapid detection of trace *Salmonella* in milk and chicken by immunomagnetic separation in combination with a chemiluminescence microparticle immunoassay. Analytical and bioanalytical chemistry.
Li, X., Li, X., Guo, Y., Liu, Y., Mei, S., Song, X., Li, J., Grugbaye, A.G., Li, J., Xu, K., 2019b. Development and Assessment of a Paper-based Enzyme-linked Immunosorbent Assay for the Colorimetric Diagnosis of Human Brucellosis. Analytical Letters 52(10), 1614-1628.
Lian, X., Fang, Y., Joseph, E., Wang, Q., Li, J., Banerjee, S., Lollar, C., Wang, X., Zhou, H.C., 2017. Enzyme-MOF (metal-organic framework) composites. Chemical Society reviews 46(11), 3386-3401.
Liang, K., Ricco, R., Doherty, C.M., Styles, M.J., Bell, S., Kirby, N., Mudie, S., Haylock, D., Hill, A.J., Doonan, C.J., Falcaro, P., 2015. Biomimetic mineralization of metal-organic frameworks as protective coatings for biomacromolecules. Nature communications 6, 7240.
Liu, Z., Yao, C., Yang, C., Wang, Y., Wan, S., Huang, J., 2018. Development of DNAzyme-based PCR signal cascade amplification for visual detection of *Listeria monocytogenes* in food. Analytical biochemistry 553, 7-11.
Lu, Z., Zhang, K., Shi, Y., Huang, Y., Wang, X., 2018. Efficient Removal of *Escherichia coli* from Ballast Water Using a Combined High-Gradient Magnetic

Separation-Ultraviolet Photocatalysis (HGMS-UV/TiO2) System. Water, Air, & Soil Pollution 229(8).

Medetalibeyoğlu, H., Manap, S., Yokuş, Ö.A., Beytur, M., Kardaş, F., Akyıldırım, O., Özkan, V., Yüksek, H., Yola, M.L., Atar, N., 2018. Fabrication of Pt/Pd Nanoparticles/Polyoxometalate/Ionic Liquid Nanohybrid for Electrocatalytic Oxidation of Methanol. Journal of The Electrochemical Society 165(5), F338-F341.

Mohamadi, R.M., Svobodova, Z., Bilkova, Z., Otto, M., Taverna, M., Descroix, S., Viovy, J.L., 2015. An integrated microfluidic chip for immunocapture, preconcentration and separation of beta-amyloid peptides. Biomicrofluidics 9(5), 054117.

Ryumae, U., Hibi, K., Yoshiura, Y., Ren, H., Endo, H., 2010. Rapid and highly sensitive detection of Flavobacterium psychrophilum using high gradient immunomagnetic separation with flow cytometry. Aquaculture 309(1-4), 125-130.

Ryumae, U., Hibi, K., Yoshiura, Y., Ren, H., Endo, H., 2012. Ultra highly sensitive method for detecting Flavobacterium psychrophilum using high-gradient immunomagnetic separation with a polymerase chain reaction. Aquaculture Research 43(6), 929-939.

Saliba, A.E., Saias, L., Psychari, E., Minc, N., Simon, D., Bidard, F.C., Mathiot, C., Pierga, J.Y., Fraisier, V., Salamero, J., Saada, V., Farace, F., Vielh, P., Malaquin, L., Viovy, J.L., 2010. Microfluidic sorting and multimodal typing of cancer cells in self-assembled magnetic arrays. Proceedings of the National Academy of Sciences of the United States of America 107(33), 14524-14529.

Schaumburg, F., Carrell, C., Henry, C.S., 2019. Rapid bacteria detection at low concentrations using sequential immunomagnetic separation and paper-based isotachophoresis. Analytical Chemistry.

Sun, J., Huang, J., Li, Y., Lv, J., Ding, X., 2019. A simple and rapid colorimetric bacteria detection method based on bacterial inhibition of glucose oxidase-catalyzed reaction. Talanta 197, 304-309.

Tan, F., Xie, X., Xu, A., Deng, K., Zeng, Y., Yang, X., Huang, H., 2019. Fabricating and regulating peroxidase-like activity of eggshell membrane-templated gold nanoclusters for colorimetric detection of staphylococcal enterotoxin B. Talanta 194, 634-642.

Tolga Çolak, A., Eren, T., Yola, M.L., Beşli, E., Şahin, O., Atar, N., 2016. 3D Polyoxometalate-Functionalized Graphene Quantum Dots with Mono-Metallic and Bi-Metallic Nanoparticles for Application in Direct Methanol Fuel Cells. Journal of The Electrochemical Society 163(10), F1237-F1244.

Vellaisamy, K., Li, G., Wang, W., Leung, C.H., Ma, D.L., 2018. A long-lived peptide-conjugated iridium(iii) complex as a luminescent probe and inhibitor of the cell migration mediator, formyl peptide receptor 2. Chemical science 9(43), 8171-8177.

Wang, C., Xing, K., Zhang, G., Yuan, M., Xu, S., Liu, D., Chen, W., Peng, J., Hu, S., Lai, W.H., 2019a. Novel ELISA based on fluorescent quenching of DNA-stabilized silver nanoclusters for detecting *E. coli* O157:H7. Food chemistry 281, 91-96.

Wang, H., Ma, Z., 2019. "Off-on" signal amplification strategy amperometric

immunosensor for ultrasensitive detection of tumour marker. Biosensors & bioelectronics 132, 265-270.

Wang, H., Tang, Z., Wang, Y., Ma, G., Tao, N., 2019b. Probing Single Molecule Binding and Free Energy Profile with Plasmonic Imaging of Nanoparticles. Journal of the American Chemical Society 141(40), 16071-16078.

Wang, K.Y., Bu, S.J., Ju, C.J., Han, Y., Ma, C.Y., Liu, W.S., Li, Z.Y., Li, C.T., Wan, J.Y., 2019c. Disposable syringe-based visual immunotest for pathogenic bacteria based on the catalase mimicking activity of platinum nanoparticle-concanavalin A hybrid nanoflowers. Mikrochimica acta 186(2), 57.

Wang, K.Y., Bu, S.J., Ju, C.J., Li, C.T., Li, Z.Y., Han, Y., Ma, C.Y., Wang, C.Y., Hao, Z., Liu, W.S., Wan, J.Y., 2018. Hemin-incorporated nanoflowers as enzyme mimics for colorimetric detection of foodborne pathogenic bacteria. Bioorganic & medicinal chemistry letters 28(23-24), 3802-3807.

Wang, L., Huang, F., Cai, G., Yao, L., Zhang, H., Lin, J., 2017. An Electrochemical Aptasensor Using Coaxial Capillary with Magnetic Nanoparticle, Urease Catalysis and PCB Electrode for Rapid and Sensitive Detection of Escherichia coli O157:H7. Nanotheranostics 1(4), 403-414.

Wang, Y., Chen, Q., Gan, C., Yan, B., Han, Y., Lin, J., 2016. A Review on Magnetophoretic Immunoseparation. Journal of Nanoscience and Nanotechnology 16(3), 2152-2163.

Wang, Y., Salazar, J.K., 2016. Culture-Independent Rapid Detection Methods for Bacterial Pathogens and Toxins in Food Matrices. Comprehensive Reviews in Food Science and Food Safety 15(1), 183-205.

Wu, C., Wu, K.J., Liu, J.B., Zhou, X.M., Leung, C.H., Ma, D.L., 2019. A dual-functional molecular strategy for in situ suppressing and visualizing of neuraminidase in aqueous solution using iridium(iii) complexes. Chemical communications 55(45), 6353-6356.

Wu, X., Yang, C., Ge, J., Liu, Z., 2015. Polydopamine tethered enzyme/metal-organic framework composites with high stability and reusability. Nanoscale 7(45), 18883-18886.

Xie, X., Tan, F., Xu, A., Deng, K., Zeng, Y., Huang, H., 2019. UV-induced peroxidase-like activity of gold nanoclusters for differentiating pathogenic bacteria and detection of enterotoxin with colorimetric readout. Sensors and Actuators B: Chemical 279, 289-297.

Yola, M.L., Atar, N., 2017. Electrochemical Detection of Atrazine by Platinum Nanoparticles/Carbon Nitride Nanotubes with Molecularly Imprinted Polymer. Industrial & Engineering Chemistry Research 56(27), 7631-7639.

Zeinhom, M.M.A., Wang, Y., Song, Y., Zhu, M.J., Lin, Y., Du, D., 2018. A portable smart-phone device for rapid and sensitive detection of *E. coli* O157:H7 in Yoghurt and Egg. Biosensors & bioelectronics 99, 479-485.

Zhu, F., Zhao, G., Dou, W., 2018. Electrochemical sandwich immunoassay for *Escherichia coli* O157:H7 based on the use of magnetic nanoparticles and graphene functionalized with electrocatalytically active Au@Pt core/shell nanoparticles. Mikrochimica acta 185(10), 455.

Figure captions

Fig. 1 Schematic of the proposed colorimetric biosensor for ultrasensitive detection of *Salmonella* from large volume of sample

Fig. 2 (a) The simulation of the magnetic field with and without the iron hoop for controlling the magnetic field lines; (b) The distribution of the magnetic field in the fluidic channel with the absence and presence of iron hoop; (c) The separation efficiency of the target bacteria with and without the iron hoop; (d) The simulation of the magnetic field using the magnets with different length; (e) The distribution of the magnetic field with different length of magnets in the fluidic channel

Fig. 3 (a) Optimization of the size of the IMPs; (b) Optimization of the flow rate of the bacterial sample

Fig. 4 (a) The color for the Pt@ZIF-8 prepared with different volume of the Pt nanoparticles; (b) Optimization of the volume of the Pt nanoparticles; (c) Optimization of the amount of the immune Pt@ZIF-8; (d) Optimization of the catalytic reaction time

Fig. 5 TEM images of the Pt (a), ZIF-8 (b) and Pt@ZIF-8 (c) nanoparticles; (d) DLS results for the ZIF-8 and Pt@ZIF-8 nanoparticles; (e) The N_2 adsorption–desorption isotherm of the ZIF-8 nanoparticles; (f) The pore size distribution of the ZIF-8 nanoparticles; (g) The absorbance for different concentrations of the Pt@ZIF-8 nanoparticles to catalyze the H_2O_2-TMB substrate.

Fig. 6 (a) The absorption spectra for different concentrations of the target bacteria; (b) Calibration curve of this proposed biosensor; (c) TEM image of the MP-bacteria and

660 MP-bacteria-Pt@ZIF-8 complexes; (d) Microscopic images of the magnetic particle
661 chains; (e) The specificity of the proposed biosensor to the non-target bacteria; (f)
662 Detection of *Salmonella* Typhimurium in chicken carcass using the proposed
663 biosensor.
664
665

666

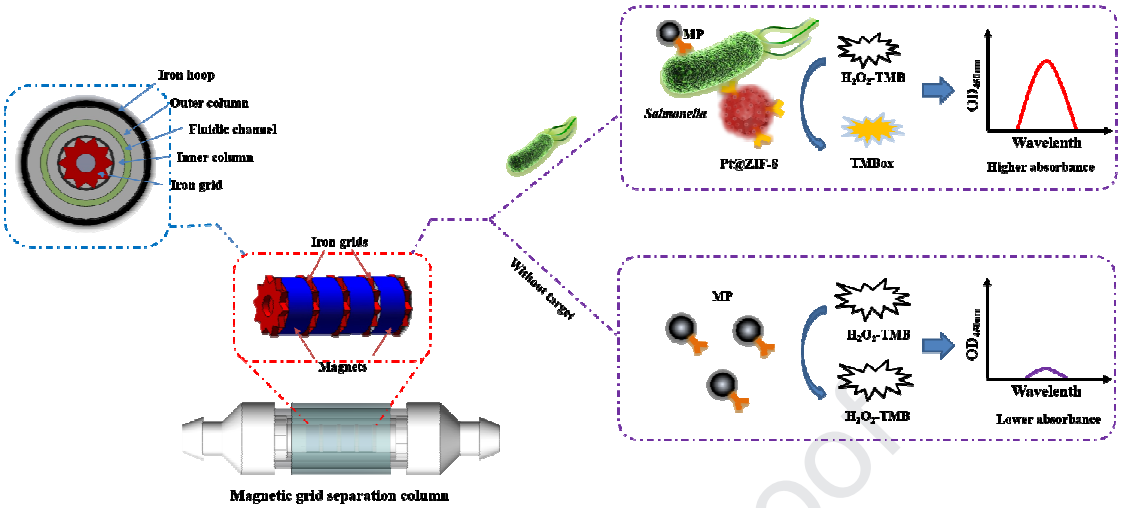

667

668

669

670 **Fig. 1**

671

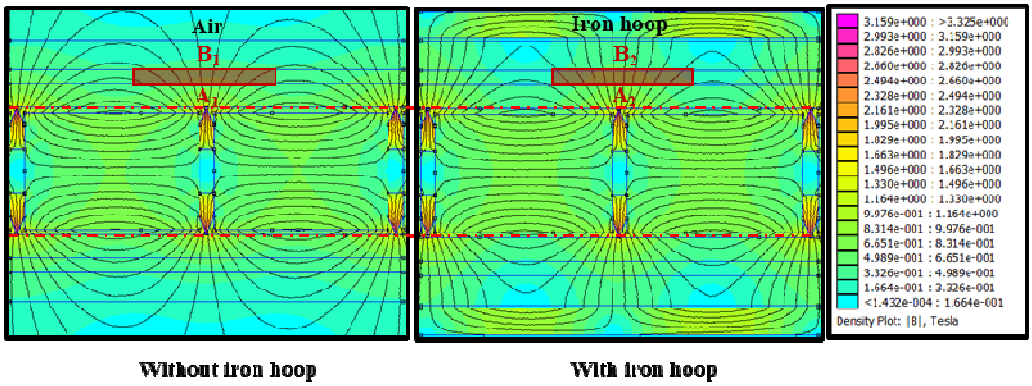
Air
B1
A1
Iron hoop
B2
A2
Density Plot: |B|, Tesla
Without iron hoop
With iron hoop

(a)

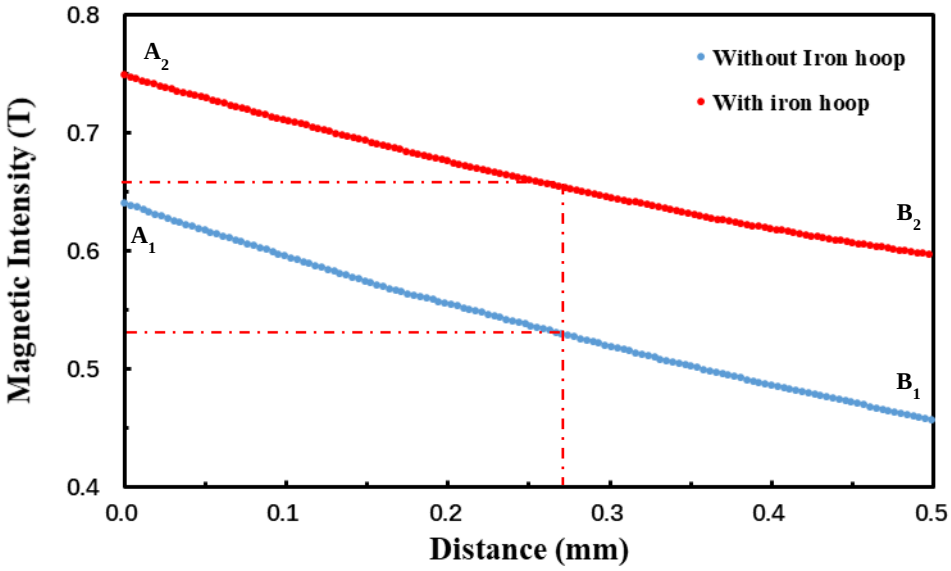
A2
A1
B2
B1
Without Iron hoop
With iron hoop
Magnetic Intensity (T)
Distance (mm)
0.8
0.7
0.6
0.5
0.4
0.0
0.1
0.2
0.3
0.4
0.5

(b)

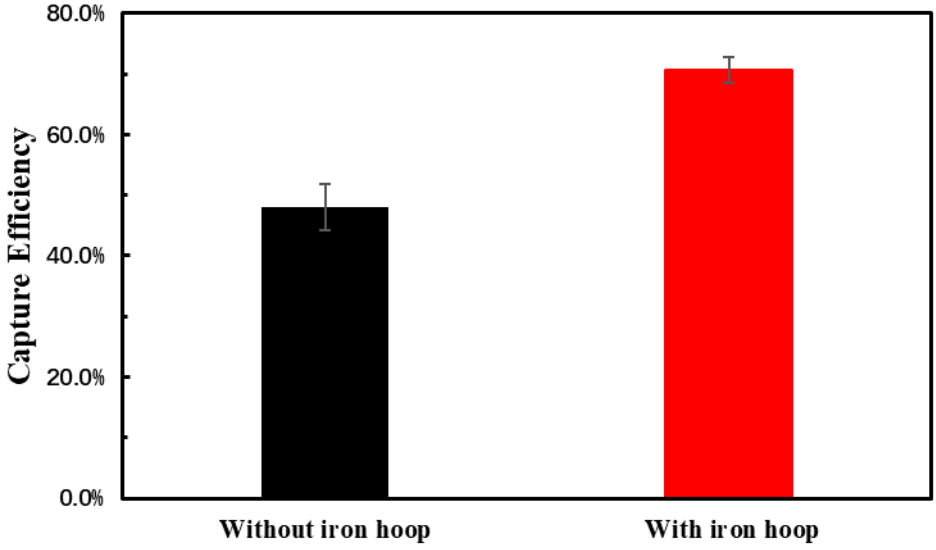
Capture Efficiency
80.0%
60.0%
40.0%
20.0%
0.0%
Without iron hoop
With iron hoop

(c)

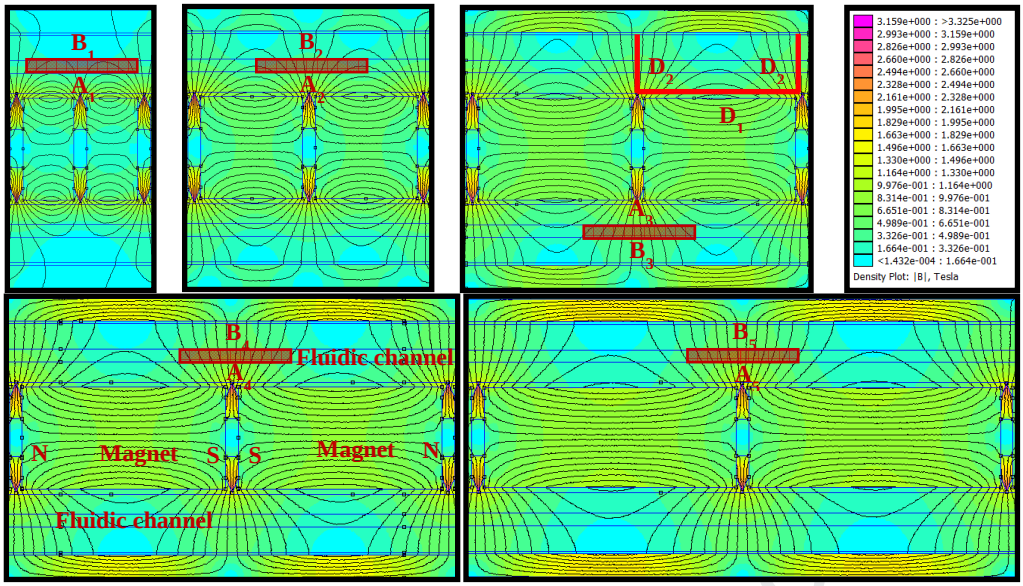
B1
A1
B2
A2
D2
D2
D1
A3
B3
3.159e+000 : >3.325e+000
2.993e+000 : 3.159e+000
2.826e+000 : 2.993e+000
2.660e+000 : 2.826e+000
2.494e+000 : 2.660e+000
2.328e+000 : 2.494e+000
2.161e+000 : 2.328e+000
1.995e+000 : 2.161e+000
1.829e+000 : 1.995e+000
1.663e+000 : 1.829e+000
1.496e+000 : 1.663e+000
1.330e+000 : 1.496e+000
1.164e+000 : 1.330e+000
9.976e-001 : 1.164e+000
8.314e-001 : 9.976e-001
6.651e-001 : 8.314e-001
4.989e-001 : 6.651e-001
3.326e-001 : 4.989e-001
1.664e-001 : 3.326e-001
<1.432e-004 : 1.664e-001
Density Plot: |B|, Tesla
B4
A4
Fluidic channel
N
Magnet
S
S
Magnet
N
Fluidic channel
B5
A5

(d)

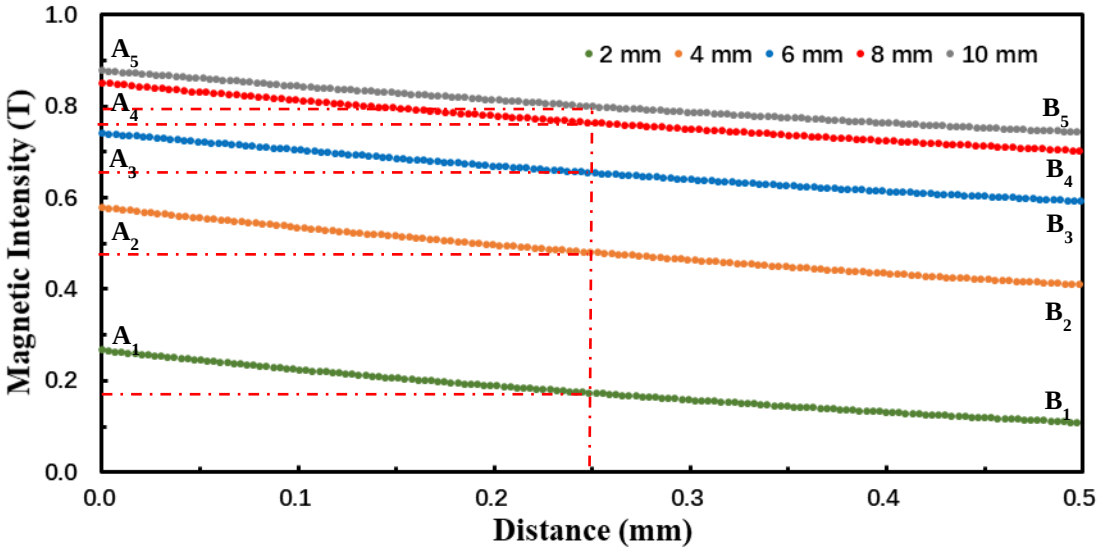
2 mm
4 mm
6 mm
8 mm
10 mm
A5
A4
A3
A2
A1
B5
B4
B3
B2
B1
Magnetic Intensity (T)
Distance (mm)
0.0
0.2
0.4
0.6
0.8
1.0
0.0
0.1
0.2
0.3
0.4
0.5

(e)

Fig. 2

687

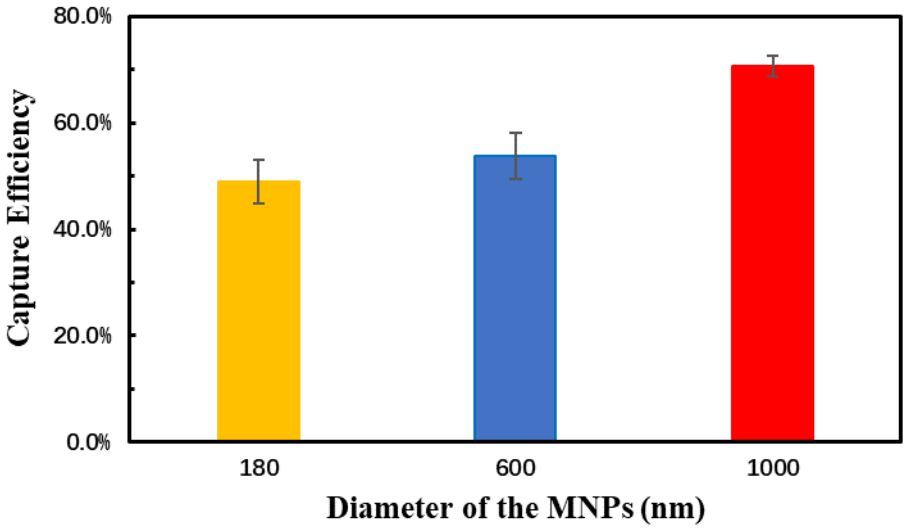

688

689 **(a)**

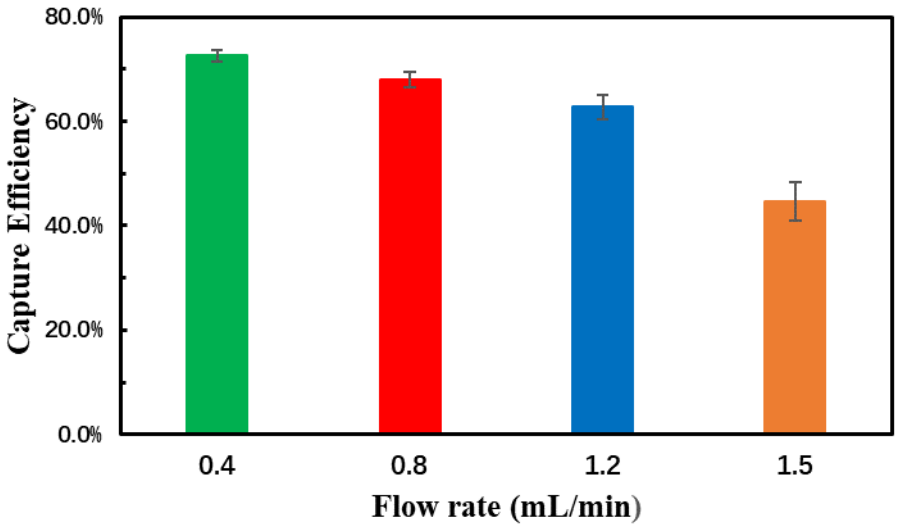

690

691 **(b)**

692

693 **Fig. 3**

694

695

696

697 **(a)**

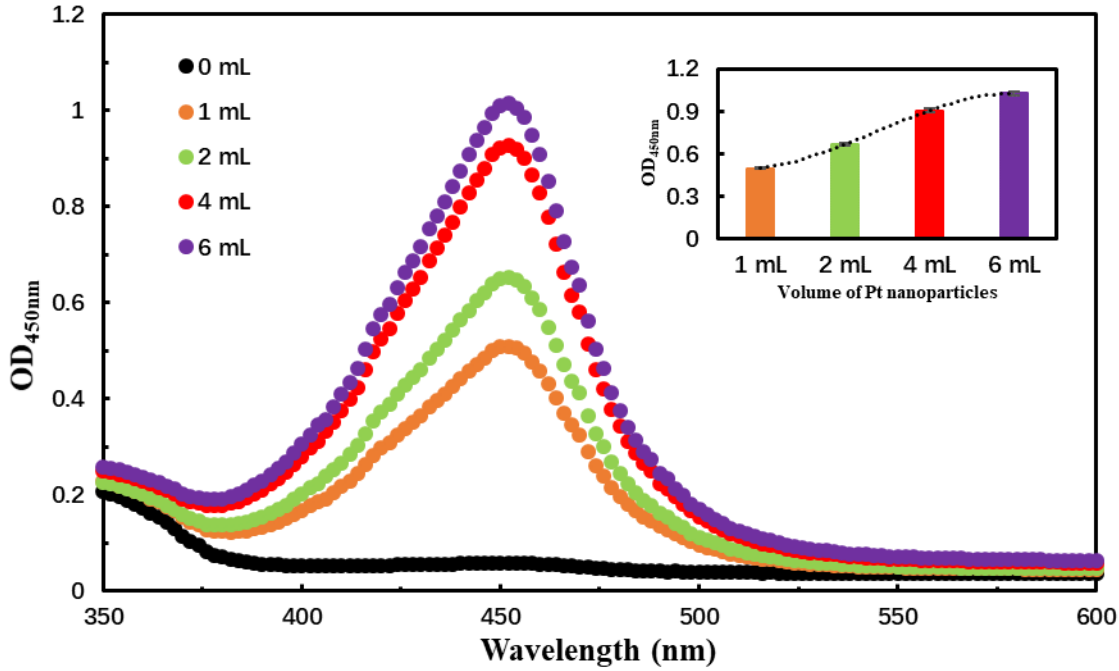

698

699 **(b)**

700

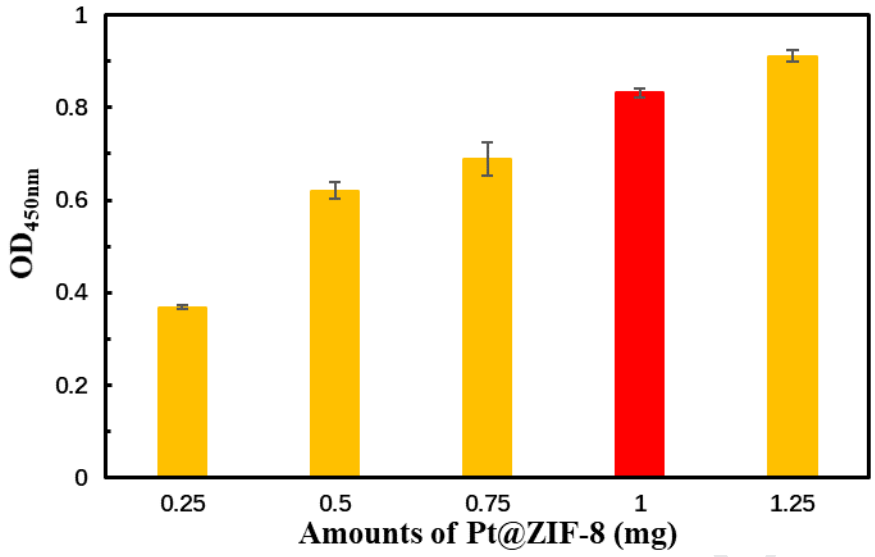
1
0.8
0.6
0.4
0.2
0
OD450nm
0.25
0.5
0.75
1
1.25
Amounts of Pt@ZIF-8 (mg)

(c)

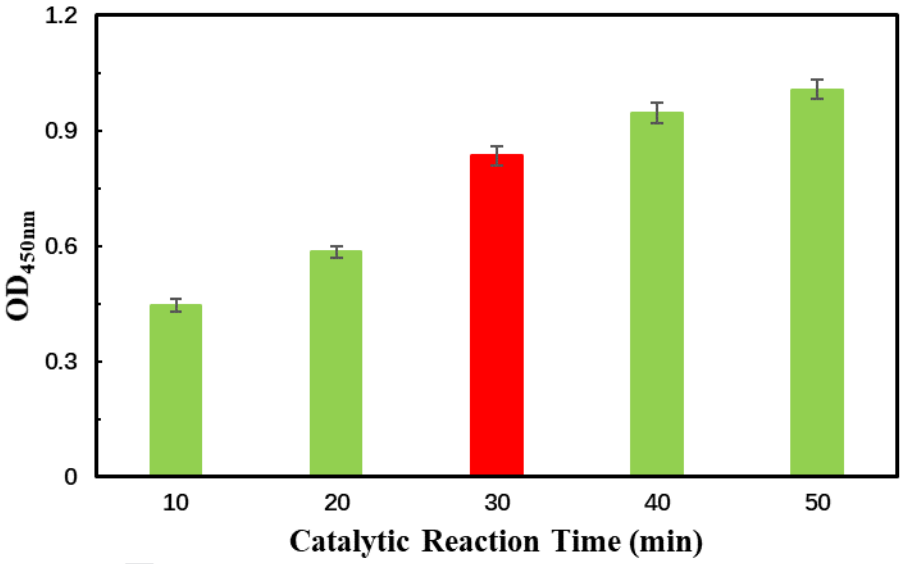
1.2
0.9
0.6
0.3
0
OD450nm
10
20
30
40
50
Catalytic Reaction Time (min)

(d)

Fig. 4

708

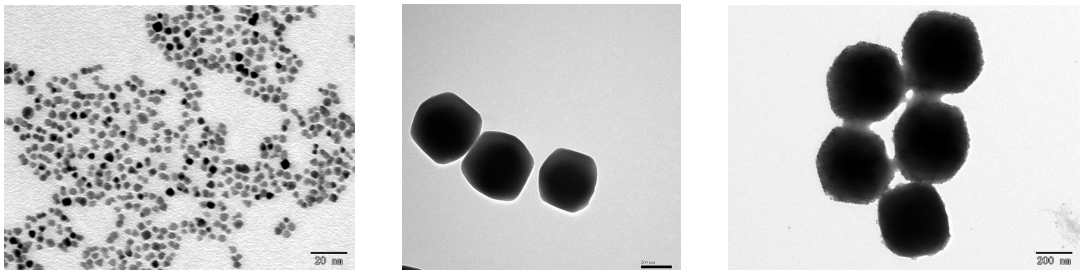

709

710 **(a)** **(b)** **(c)**

711

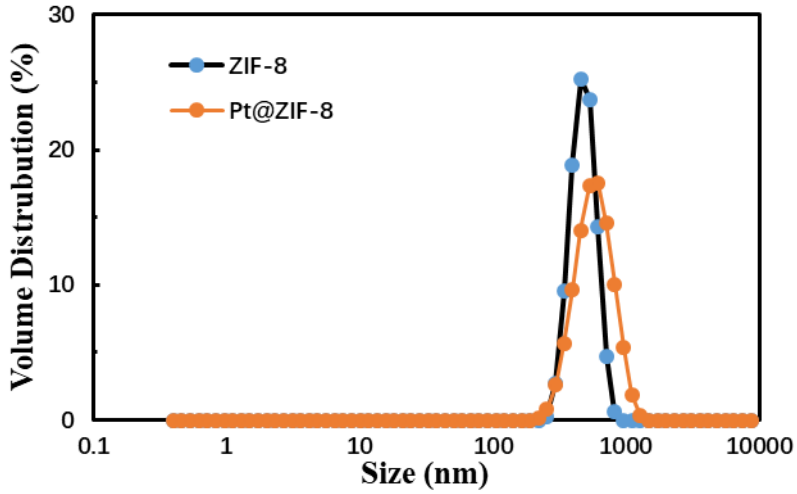

712

713 **(d)**

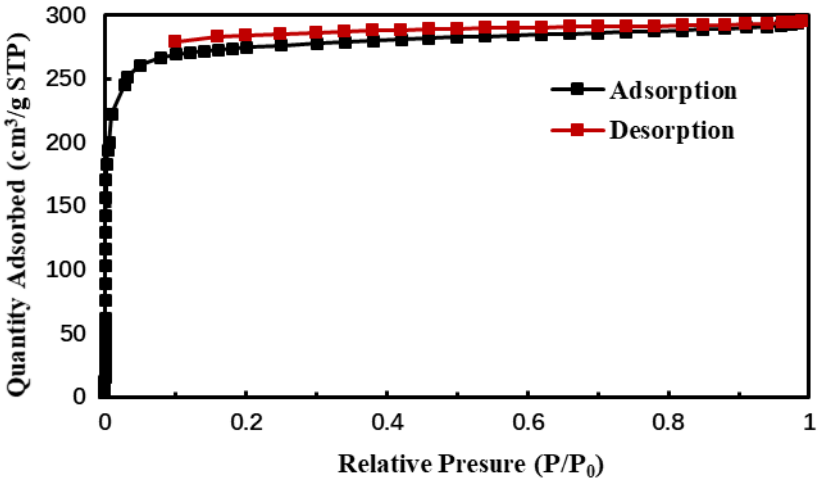

714

715 **(e)**

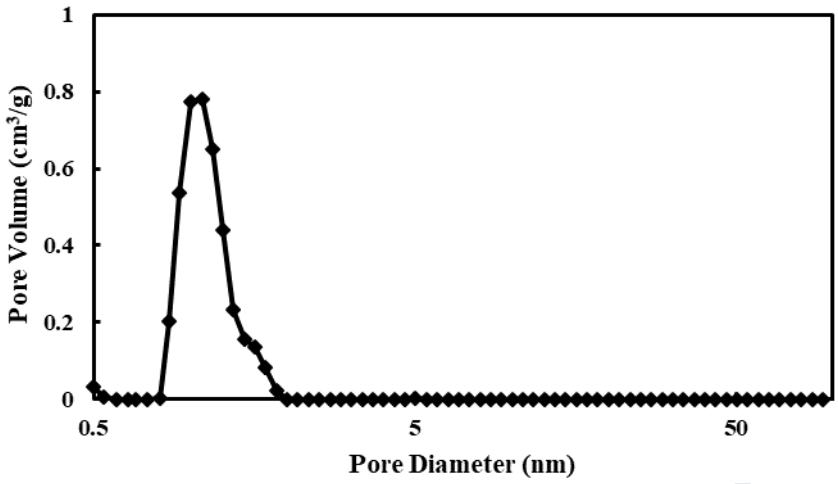

716

717 **(f)**

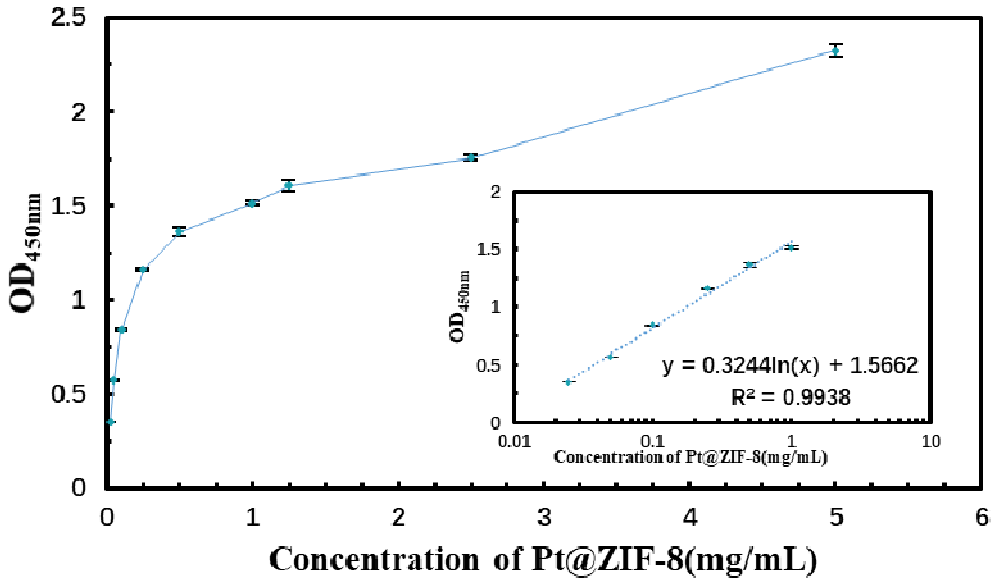

718

719 **(g)**

720

721 **Fig. 5**

722

723

724

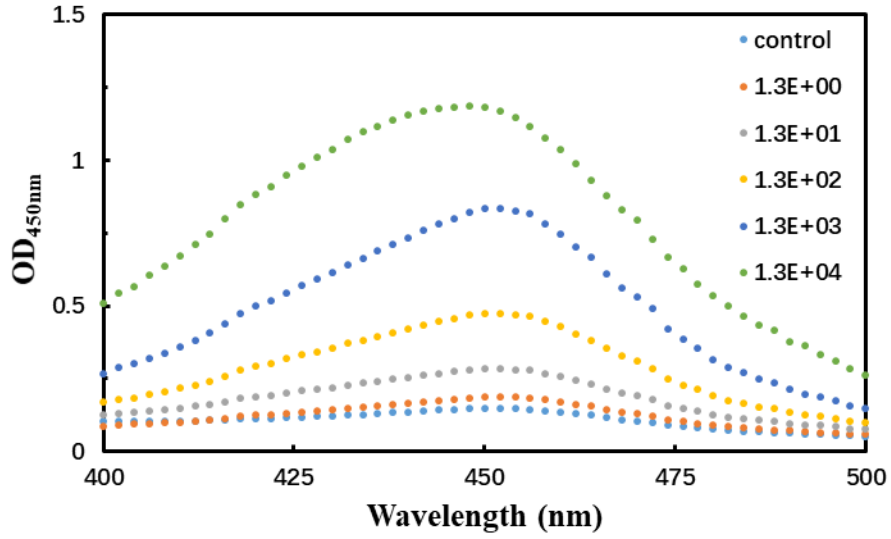

725

726 **(a)**

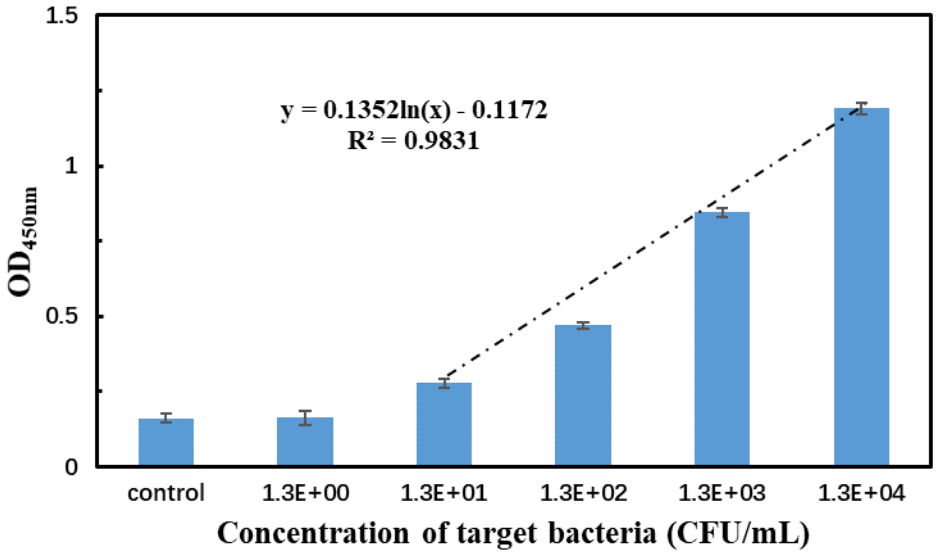

727

728 **(b)**

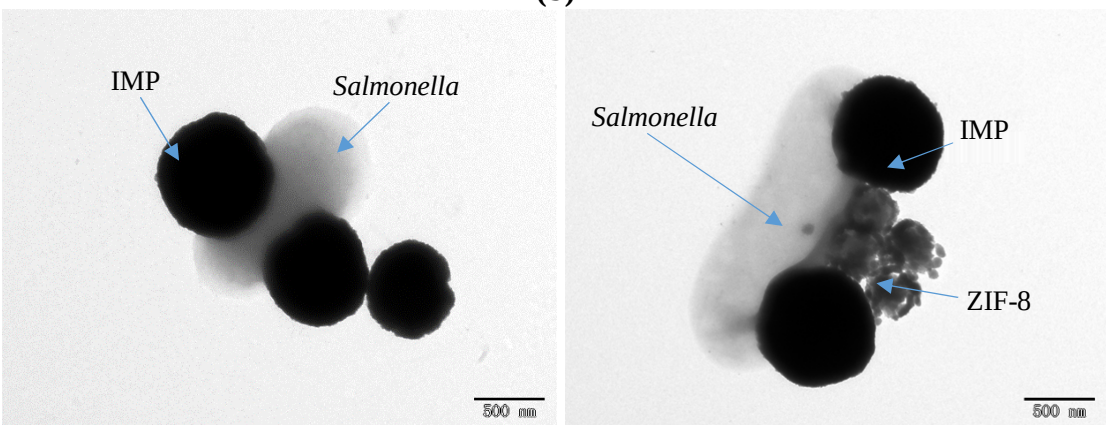

729

730 **(c)**

731

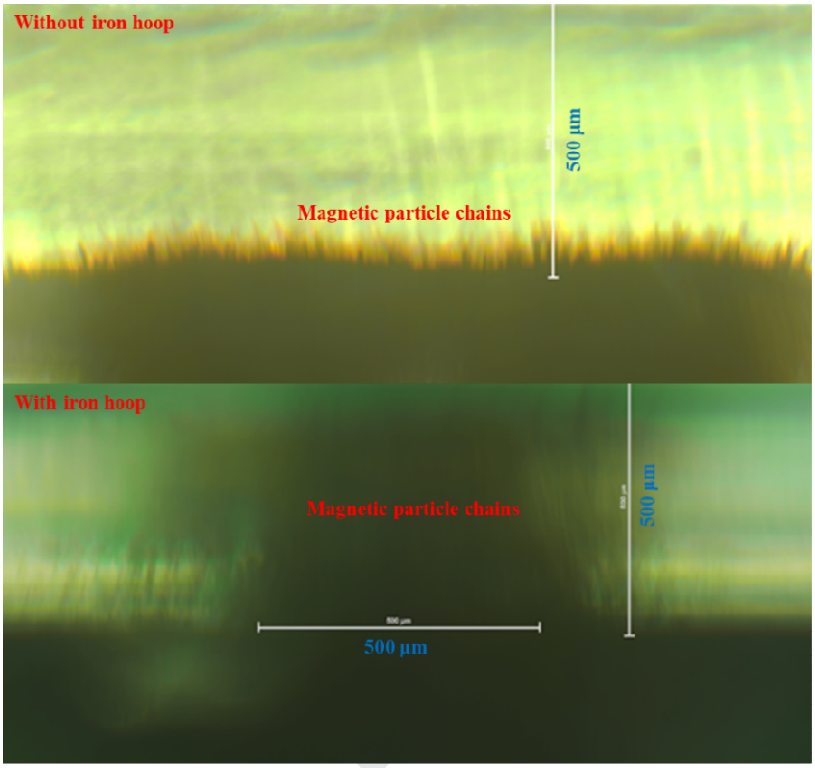

732

733 **(d)**

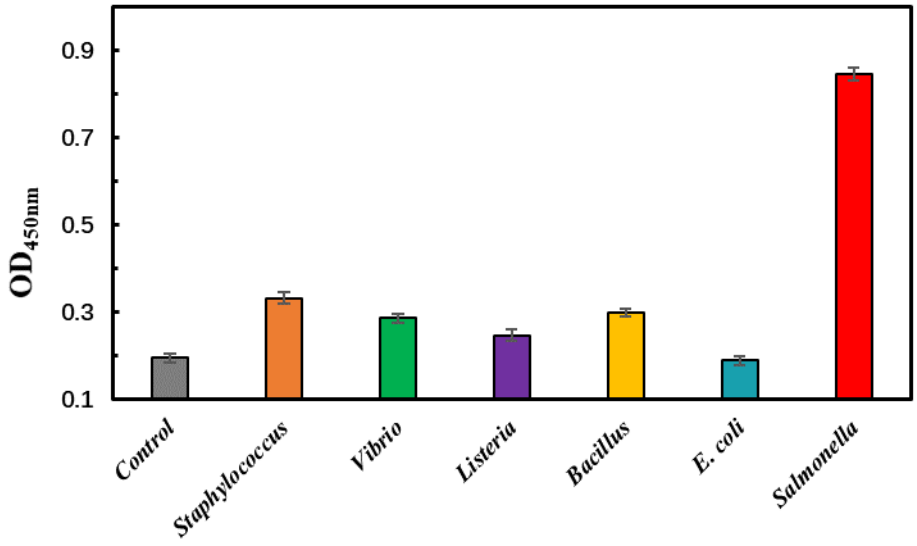

734

735 **(e)**

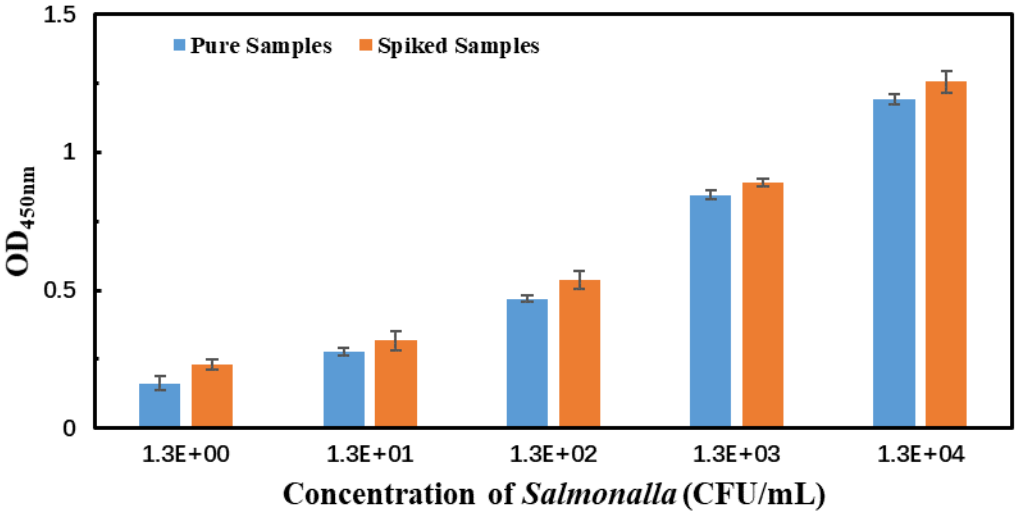

736

737 **(f)**

738

739 **Fig. 6**

Highlights

Magnetic particle chains were successfully formed in fluidic channel using iron grid.

Magnetic grid separation was very effective to separate target bacteria from large volume.

Pt@ZIF-8 with HRP-mimic enzymatic activity could greatly amplify biological signals.

This biosensor was able to detect *Salmonella* as low as 2 CFU/mL in 2.5 h.

This biosensor might be used for bacterial routine screening without any pre-enrichment.

Author Contribution Statement

Lei Wang contributed to Conceptualization, Methodology, Formal analysis, Resources, Validation, Writing-Original Draft.

Xiaoting Huo contributed to Investigitation, Visualization.

Lingyan Zheng contributed to Resources.

Gaozhe Cai and **Yuhe Wang** contributed to Methodology.

Ning Liu contributed to Validation.

Maohua Wang contributed to Supervision.

Jianhan Lin contributed to Conceptualization, Data Curation, Writing- Reviewing and Editing, Project administration, Funding acquisition

Conflict of interest

☒ The authors declare that they have no conflicts of interest.

☐ The authors declare the following conflicts of interest:

CRediT author statement

Lei Wang: Conceptualization, Methodology, Formal analysis, Resources, Validation, Writing-Original Draft

Xiaoting Huo: Investigitation, Visualization

Lingyan Zheng: Resources

Gaozhe Cai: Methodology

Yuhe Wang: Methodology

Ning Liu： Validation

Maohua Wang： Supervision

Jianhan Lin: Conceptualization, Data Curation, Writing- Reviewing and Editing, Project administration, Funding acquisition

Declaration of interests

☒ The authors declare that they have no known competing financial interests or personal relationships that could have appeared to influence the work reported in this paper.

☐The authors declare the following financial interests/personal relationships which may be considered as potential competing interests: